How to cite: *Angew. Chem. Int. Ed.* **2024**, *63*, e202411044
doi.org/10.1002/anie.202411044

VIP **Solar Cells** *Very Important Paper*

Isomeric Dimer Acceptors for Stable Organic Solar Cells with over 19 % Efficiency

Yun Li, Zhongwei Ge, Le Mei, Haisheng Ma, Yue Chen, Xunchang Wang, Jifa Yu, Guanghao Lu, Renqiang Yang, Xian-Kai Chen, Shouchun Yin, and Yanming Sun**

Abstract: The strategy of isomerization is known for its simple yet effective role in optimizing molecular configuration and enhancing the power conversion efficiency (PCE) of organic solar cells (OSCs). However, the impact of isomerization on the design of dimer acceptors has been rarely investigated, and the relationship between the chemical structure and optoelectronic property remains unclear. In this study, we designed and synthesized two dimer acceptor isomers named D-TPh and D-TN, which differ in the positional arrangement of their end capping groups. Compared to D-TN, D-TPh exhibited enhanced backbone planarity, elevated lowest unoccupied molecular orbital energy level, and more ordered molecular stacking. Consequently, the OSC device based on PM6:D-TPh achieved a PCE of 19.05 %, higher than that (PCE = 18.42 %) of the device based on PM6:D-TN. Large-area PM6:D-TPh devices (1 cm^2) yielded a PCE of 18.00 %. More importantly, the extrapolated T_{80} lifetime of the PM6:D-TPh device is over 2800 h with MPP tracking under continuous one-sun illumination. These results suggest that isomerization strategy is an effective way to optimize the molecular configuration of dimer acceptors for the fabrication of high-efficiency and stable OSCs.

Introduction

Organic solar cells (OSCs) are regarded as promising renewable and eco-friendly energy sources due to their distinctive benefits, including light weight, cost-effectiveness, sustainable printability, and potential for flexibility.[1–5] The power conversion efficiency (PCE) of OSCs has been significantly improved, largely due to advancements in non-fullerene acceptors.[6–8] However, devices that utilize small molecule acceptors (SMAs) are prone to morphological degradation,[9] which adversely impacts long-term stability of OSCs.[10–11] To address this issue, it is essential to develop innovative materials with lower diffusion properties to slow down the degradation of the active layer.[12]

Dimer acceptors consisting of two SMA units have definite molecular structure and remarkable excellent batch-to-batch reproducibility.[13–14] Furthermore, the dimer acceptors, with more extended molecular lengths compared with the SMAs, can also have significantly higher glass transition temperature (T_g), facilitating the achievement of an optimal kinetic morphology,[15] which has proven to be an effective strategy for enhancing both the PCE and stability of OSCs.[16–21] Isomers, which are substances with the same molecular formula but distinct chemical and physical properties,[22–23] have emerged as a promising strategy for enhancing the efficiency of OSCs.[24] This is achieved through the rational tuning of molecular structures to precisely adjust the electronic structure, absorption spectra, charge transport properties, and molecular stacking, all of which are pivotal to device performance.[25–29] Much effort has been focused on investigating the effect of isomeric end capping groups or side chains on the properties of Y6-derivatives.[30–34] However, study on dimer acceptors has been rarely reported. Consequently, there is significant potential for the development of novel dimer acceptor isomers. Such advancements could provide a deeper under-

[*] Y. Li, Prof. S. Yin
Key Laboratory of Organosilicon Chemistry and Materials Technology of Ministry of Education,
College of Materials, Chemistry and Chemical Engineering,
Hangzhou Normal University, Hangzhou, P. R. China
E-mail: yinsc@hznu.edu.cn

Y. Li, Z. Ge, H. Ma, Y. Chen, Prof. Y. Sun
School of Chemistry
Beihang University
Beijing 100191, P. R. China
E-mail: sunym@buaa.edu.cn

L. Mei, Prof. X.-K. Chen
Institute of Functional Nano & Soft Materials (FUNSOM), Jiangsu Key Laboratory of Advanced Negative Carbon Technologies,
Soochow University
Suzhou, 215123, Jiangsu, P. R. China

L. Mei
Department of Chemistry
City University of Hong Kong
Kowloon, Hong Kong, 999077, P. R. China

Dr. X. Wang, Prof. R. Yang
Key Laboratory of Optoelectronic Chemical Materials and Devices (Ministry of Education), School of Optoelectronic Materials & Technology
Jianghan University
Wuhan 430056, P. R. China

J. Yu, Prof. G. Lu
Institute of Science and Technology,
Xi'an Jiaotong University,
Xi'an 710054, China

standing of the relationship between molecular structure and properties, ultimately contributing to the realization of high-performance and stable OSCs.

Dimer acceptors are predominantly synthesized through Stille coupling reactions, which involve an asymmetric monobrominated monomer and a diorganotin-functionalized linker.[35] The asymmetric monobrominated monomers are typically produced via a one-pot Knoevenagel condensation reaction between a dialdehyde intermediate and two distinct end-groups, such as IC-2H (2-(3-oxo-2,3-dihydro-1*H*-inden-1-ylidene) malononitrile) and IC-γ-Br (2-(5-bromo-3-oxo-2,3-dihydro-1*H*-inden-1-ylidene) malononitrile).[36] However, these one-pot approach encounters have some challenges, including moderate yields and complex separation processes.[37] To address the challenges, we utilize two end-groups with significant structural differences: NIC-2F(2-(6,7-difluoro-3-oxo-2,3-dihydro-1*H*-cyclopenta[b]naphthalen-1-ylidene) malononitrile) and IC-γ-Br. The distinct structures facilitate the separation process and can potentially increase the yield of monomers to over 60 %, which is a substantial improvement over the typical range of 30–40 %. We have also synthesized an isomer monomer using NIC-γ-Br (2-(6-bromo-3-oxo-2,3-dihydro-1*H*-cyclopenta[b]naphthalen-1-ylidene) malononitrile) and IC-2F(2-(5,6-difluoro-3-oxo-2,3-dihydro-1*H*-inden-1-ylidene) malononitrile) as the end-groups. Herein, we designed and synthesized two dimer acceptors, D-TPh and D-TN, which differ in the positional arrangement of end capping groups. When blended with PM6, OSCs based on D-TPh and D-TN demonstrated high photovoltaic performance. Specifically, the device based on PM6:D-TPh achieved a remarkable PCE of 19.05 %, with an open-circuit voltage (V_{oc}) of 0.946 V, a short-circuit current density (J_{sc}) of 25.59 mA cm^{-2}, and a fill factor (FF) of 78.7 %. In contrast, PM6:D-TN-based device showed a slightly lower PCE of 18.42 %. Notably, large-area (1 cm^2) devices based on PM6:D-TPh achieved a high efficiency of 18.00 %. Furthermore, these dimers exhibits a high T_g, coupled with low kinetic disorder, leading to superior thermal and long-term stability. The device based on PM6:D-TN maintained over 80 % of its initial PCE after 680 h of continuous heating at 80 °C, and the device displayed a reduced efficiency drop, with its extrapolated T_{80} lifetime significantly extended to 2800 h with maximum power point (MPP) tracking under continuous one-sun illumination. This work demonstrates that high-performance dimerized acceptors can be achieved through rational molecular structure design, specifically by employing an isomeric strategy. This approach presents a promising path towards the development of OSCs with high efficiency and long-term stability.

Results and Discussion

Materials Synthesis and Characterization

The molecular configurations of PM6 and the innovatively-engineered dimeric acceptors, designated as D-TPh and D-TN, are depicted in Figure 1a. D-TPh and D-TN are isomers, achieving through the ingenious modulation of the positions of naphthyl end-group and phenyl end-group. The detailed synthetic routes for D-TPh and D-TN are outlined in Schemes S1 and S2 (Supporting Information). The L8-BO-DT core, featuring naphthyl and phenyl end-groups,

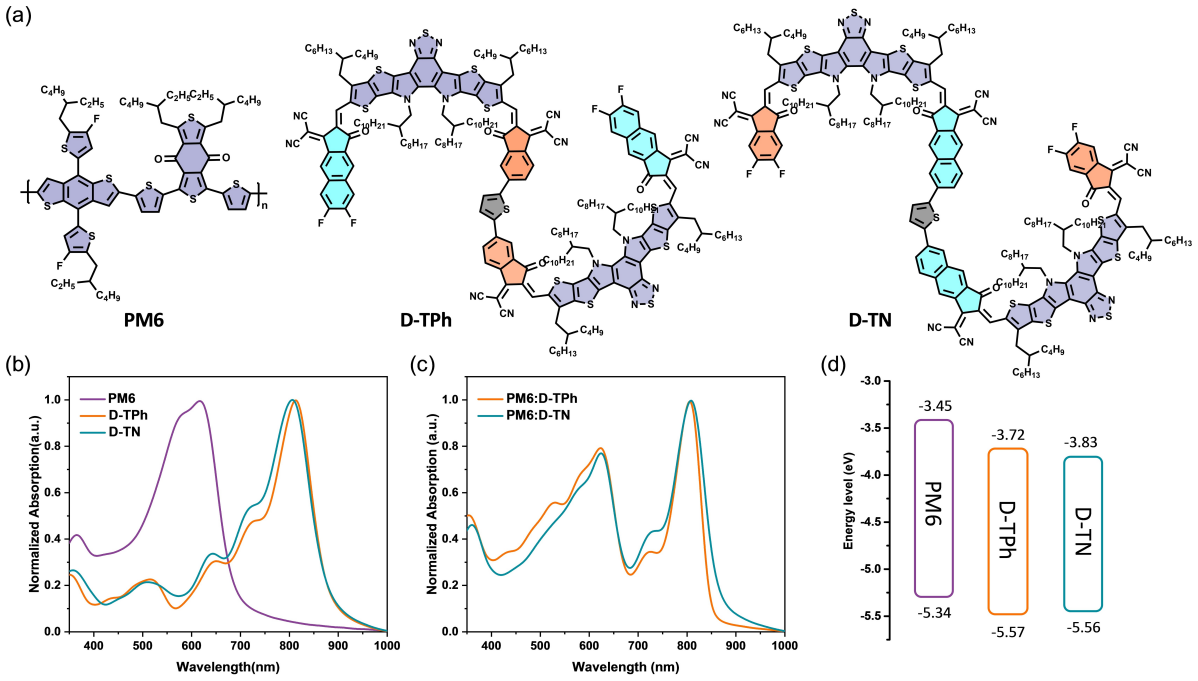

Figure 1. (a) Chemical structures of PM6, D-TPh and D-TN. (b) Normalized absorption spectra of PM6, D-TPh and D-TN films. (c) Normalized absorption spectra of PM6:D-TPh and PM6:D-TN blend films. (d) The energy-level diagram of PM6, D-TPh and D-TN.

served as the fundamental monomers, with thiophene being integrated as the π-conjugated bridging spacer. Due to the significant differences in the chemical structures of naphthyl and phenyl end-groups, the synthesis of monomers capped with these end-groups facilitates the separation of products and yields a higher production rate over 60 % (typical range of 30–40 %). The molecular configurations of D-TPh and D-TN were characterized by ^{1}H nuclear magnetic resonance (NMR) and mass spectra (MALDI-TOF) with the results depicted in Figures S1–S4. These dimeric acceptors exhibit favorable miscibility in prevalent solvents such as chloroform, toluene, and chlorobenzene, facilitating the process of device fabrication.

To examine the light absorption properties of these two dimeric acceptors, both diluted chloroform solution and film were analyzed. As shown in Figure S5, in the solution state, D-TPh and D-TN exhibit comparable light absorption patterns, reaching their peak absorption (λ_{max}) at 755 and 750 nm, respectively. In thin film (Figure 1b), a notable redshift is detected for these two acceptors, suggesting enhanced intermolecular interactions. The λ_{max} wavelengths for D-TPh and D-TN are found to be 813 and 806 nm, respectively, and they exhibit absorption within the range of 350–950 nm, which complements the absorption spectrum of PM6. As depicted in Figure 1c, the absorption of blend films nearly encompasses the entire solar spectrum from 300–950 nm. The broad absorption range ensures efficient photocurrent generation in the corresponding OSC devices. Subsequently, cyclic voltammetry (CV) assessments were conducted to obtain the energy levels of PM6 and two acceptors (Figure S6). As depicted in Figure 1d, the lowest unoccupied molecular orbital (LUMO) and the highest occupied molecular orbital (HOMO) for PM6, D-TPh and D-TN are recorded as −3.45/-5.34, −3.72/−5.57, and −3.83/−5.56, respectively. Moreover, the elevated LUMO energy level of D- TPh is anticipated to contribute to a higher V_{oc} in the related OSC device.

In order to explore the impact of isomerization on the planarity of the backbone in dimer acceptors, we conducted simulations using Density Functional Theory (DFT) at the B3LYP/6-31G level. To facilitate the calculation process, all alkyl groups were simplified to be methyl groups. As shown in Figure 2a, the simulations revealed that both dimer acceptors demonstrated planar molecular conformations, between the 1,1-dicyanomethylene-3-indanone(IC)/2-(6,7-difluoro-3-oxo-2,3-dihydro-1*H*-cyclopenta[b]naphthalen-1-ylidene)malononitrile (NIC) and the thiophene linker units within their backbones. Specifically, the average dihedral angles (θ_{avg}) for the two sides of the linker units are 33.5° for D-TPh and 36.5° for D-TN. The reduction in these θ_{avg} values for D-TPh indicates an enhancement in the planarity of the dimer acceptors' backbones. This increased planarity is advantageous as it promotes a well-ordered intermolecular assembly, which is crucial for achieving high electron mobility in films. We conducted all-atom molecular dynamics (AA-MD) simulations on PM6/D-TPh and PM6/D-TN blend films to explore the impact of different acceptors on the kinetics of the blend film formation. As shown in Figure 2b, the calculated interaction energy (the sum of Van der Waals forces) for PM6/PM6 and PM6/acceptor is

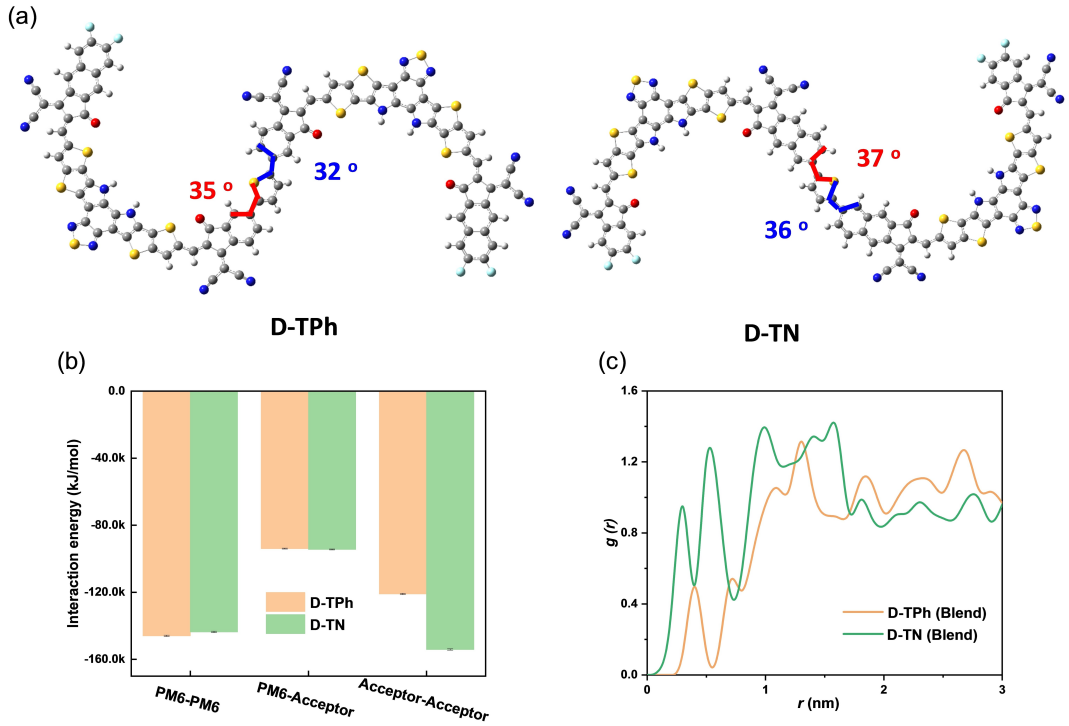

Figure 2. (a) Optimized molecular conformations and dihedral angles of the dimer acceptors obtained from DFT simulations; (b) The calculated interaction energy (the sum of Van der Waals forces) for PM6/PM6, PM6/acceptor and acceptor/ acceptor. (c) Radial distribution functions *g(r)* for D-TPh and D-TN in blend films.

comparable. However, the interaction energy for D-TN/D-TN molecules is relatively stronger than that of D-TPh/D-TPh molecules, suggesting that D-TN has a higher degree of aggregation in the mixed film than D-TPh, which is unfavorable for rational morphology. To quantitatively evaluate the stacking level in the pure film, we utilized the radial distribution function (RDF), focusing on the *g(r)* parameter. This metric allows us to determine the probability of finding a particle at a specific distance from a reference particle. The position of the first peak in the RDF signifies the mean distance separating a central particle from its nearest neighbor, embodying the equilibrium coordination distance characteristic of these particle pairs. Further, the height of this initial peak illuminates the density or count of nearest neighbor particles encircling the central particle, serving as an indicator of the strength of interparticle interactions. A taller peak height implies a greater abundance of nearest neighbors surrounding the central particle, indicative of a stronger interaction force among particles. As indicated in Figure 2c, the position of the first RDF peak for D-TN, at 0.3 nm, exhibits a notable shift towards a shorter distance compared to that of D-TPh, which stands at 0.4 nm. Furthermore, the intensity of this peak for D-TN, measured at 0.95, is significantly higher than that of D-TPh, which registers at 0.5, underscoring a stronger interaction or higher density of nearest neighbors in the case of D-TN. This finding is in perfect alignment with the results of the interaction energy analysis.

Table 1: Summary of device parameters of the devices.

Active layer	V_{oc} (V)	J_{sc} (mA cm^{-2})	FF (%)	PCE[a] (%)
PM6:D-TPh	0.946 (0.945 ± 0.001)	25.59 (25.27 ± 0.30)	78.7 (77.8 ± 0.8)	19.05 (18.87 ± 0.20)
PM6:D-TN	0.930 (0.928 ± 0.002)	25.33 (25.00 ± 0.33)	78.2 (77.1 ± 1.0)	18.42 (18.20 ± 0.23)

[a] The average parameters were calculated from 20 devices.

Photovoltaic Performances

In order to assess the efficiency of the photovoltaic properties for the dimeric acceptors, D-TPh and D-TN-based OSCs were constructed utilizing a standard architecture consisting of indium tin oxide (ITO)/2-(9*H*-carbazol-9-yl)ethyl]phosphonic acid (2PACz)/active layer/(9,9-bis(3′-(*N*,*N*-dimethylamino) propyl)-2,7-fluorene)-*alt*-5,50-bis(2,20-thiophene)-2,6-naphthalene-1,4,5,8-tetracaboxylic-*N*,*N*′-di(2-ethylhexyl) imide (PNDIT-F3N)/Ag. The detailed device preparation process can be found in the Supporting Information, while the photovoltaic parameters are summarized in Table 1. The representative current-density versus voltage (*J*–*V*) characteristics of the optimized devices under simulated AM 1.5G illumination at 100 mW cm^{-2} are presented in Figure 3a. Notably, the optimized devices utilizing the PM6:D-TPh blend demonstrated a high efficiency of

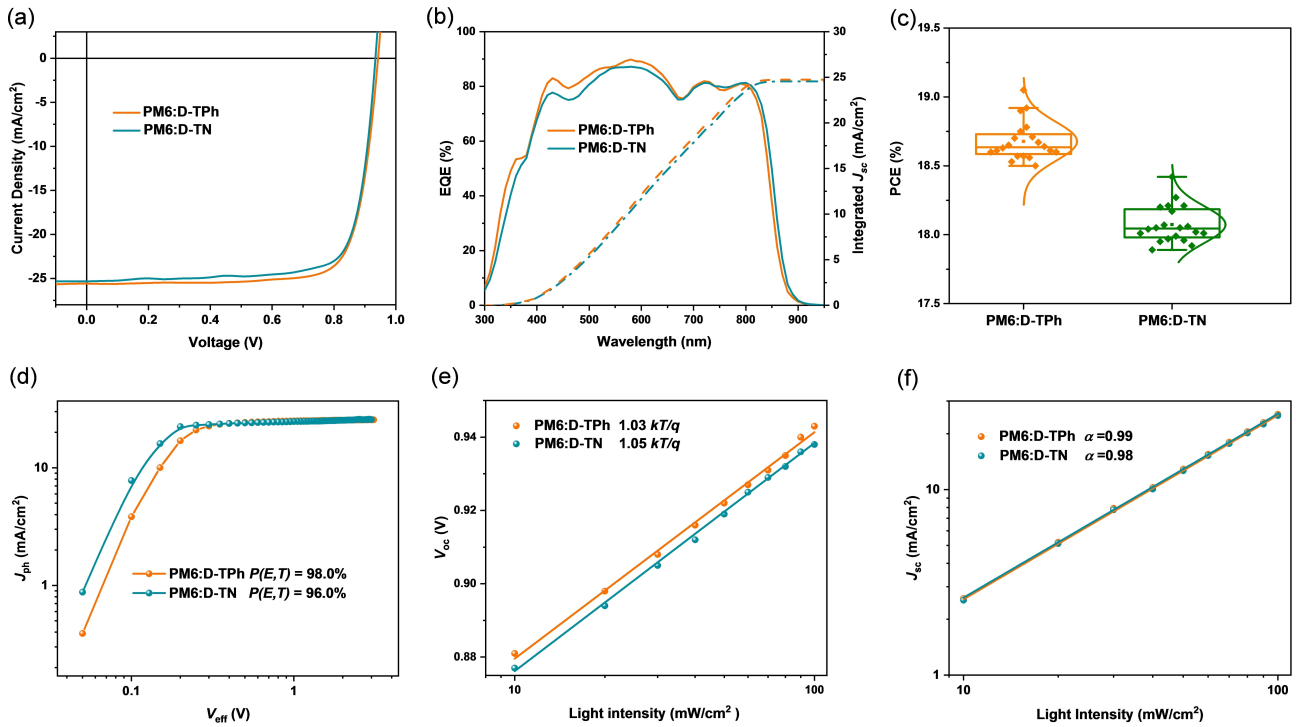

Figure 3. (a) *J*–*V* characteristics of PM6:D-TPh and PM6:D-TN devices under simulated AM 1.5G illumination at 100 mW cm^{-2}. (b) EQE spectra (solid lines) and the integrated J_{sc}s (dashed lines) of PM6:D-TPh and PM6:D-TN devices. (c) Statistical histograms of PCEs of PM6:D-TPh and PM6:D-TN devices. (d) Photocurrent density (J_{ph}) as a function of effective bias (V_{eff}) for PM6:D-TPh and PM6:D-TN devices. (e) V_{oc} versus light intensity of PM6:D-TPh and PM6:D-TN devices. (f) J_{sc} versus light intensity of PM6:D-TPh and PM6:D-TN devices.

19.05 %, attributed to the high V_{oc} of 0.946 V, a substantial J_{sc} of 25.59 mA cm^{-2}, and an impressive FF of 78.7 %. In contrast, the PM6:D-TN-based device achieved a PCE of 18.42 % with a V_{oc} of 0.930 V, with a high J_{sc} of 25.33 mA cm^{-2} and an FF of 78.2 %. Additionally, it is imperative to note that within the dimeric acceptors system, a high V_{oc} of 0.946 V and a high J_{sc} of 25.52 mA cm^{-2} have been obtained simultaneously, contributing to a record high PCE of 19.05 % for dimer acceptor-based binary OSCs. For comparison, we also fabricated devices using the monomers as the reference (Figure S7 and Table S1). It can be found that both the devices based on monomers of N-2F and N-Br exhibited V_{oc} values of 0.930 V and 0.917 V, which leads to relatively low PCEs of 18.76 % and 18.02 %, respectively. Such results support the conclusion that dimerization is an effective strategy for enhancing the performance of OSCs. Furthermore, ternary OSCs were prepared by incorporating dimers into the PM6:L8-BO system. As a result, the device based on PM6:L8-BO:D-TPh blend achieved a PCE of 19.42 % with an improved V_{oc} (Figure S8 and Table S2). The external quantum efficiency (EQE) spectra and the calculated J_{sc} values are 24.73 and 24.54 mA cm^{-2} for PM6:D-TPh and PM6:D-TN based devices, respectively (Figure 3b). It is observed that the calculated J_{sc} values align well with the results obtained from the *J–V* measurements. Particularly, in the spectral range of 300–670 nm, there is a significant enhancement in the EQE response for device based on PM6:D-TPh, providing a clear rationale for the increased J_{sc} in the OSCs.Figure 3c presents the statistical distribution of PCEs for these OSCs, further substantiating the repeatability and reliability of their high-performance characteristics. In addition, large-area devices (with an area of 1 cm^2) was fabricated to evaluate the potential for practical application. As depicted in Figure S9 and outlined in Table S3, the large-area PM6:D-TPh OSC yielded a commendable PCE of 18.00 %, with a V_{oc} of 0.959 V, a J_{sc} of 26.54 mA cm^{-2}, and an FF of 70.7 %. These results indicate the suitability of the dimeric acceptor for larger-area fabricating, offering a promising pathway for the transition from laboratory development to factory of OSCs.

Investigations of the exciton dissociation, and recombination characteristics of these dimer acceptor-based OSCs have been performed. By examining the photocurrent density (J_{ph}) in relation to the effective voltage (V_{eff}),[38] as illustrated in Figure 3d, it was observed that J_{ph} exhibited a swift rise with an increase in V_{eff} at lower voltage thresholds, eventually leveling off at approximately 2 V. The calculated *P(E,T)* values for the devices based on PM6:D-TPh and PM6:D-TN were determined to be 98.0 % and 96.0 %, respectively. The superior *P(E,T)* values of PM6:D-TPh-based devices suggest a more effective exciton dissociation at the interface between the donor and acceptor materials. Furthermore, the charge recombination within these devices were examined by analyzing the V_{oc} varies with the intensity of light (P_{light}). In the case where bimolecular recombination significantly contributes to the device's behavior, the gradient of the V_{oc} plotted against the natural logarithm of P_{light} should be equivalent to the ratio of kT/q (k is the Boltzmann constant, T is temperature, and q is elementary charge). A relationship between V_{oc} and P_{light}, surpassing the threshold of $kT/q(>kT/q)$, is indicative of trap-assisted recombination being the primary mechanism at play.[39] As presented in Figure 3e, the slopes derived from the V_{oc} versus P_{light} for devices based on PM6:D-TPh and PM6:D-TN are determined to be 1.03 and 1.05 kT/q, respectively. These results suggest that the presence of trap-assisted recombination is significantly mitigated in the PM6:D-TPh device. In addition, the examination of the J_{sc} in relation to P_{light} was conducted to gain further insights into the charge recombination dynamics within these OSCs. The correlation between J_{sc} and P_{light} is typically described by the equation $J_{sc} \propto P_{light}^{\alpha}$, with α representing the slope of the curve. An α value approaching 1 implies a suppressed bimolecular recombination under short-circuit conditions. As illustrated in Figure 3f, the determined α values for OSCs based on PM6:D-TPh and PM6:D-TN are 0.99 and 0.98, respectively. The obtained values indicate a greater reduction of bimolecular recombination in the PM6:D-TPh-based OSC, leading to an improved FF.

To determine the charge transport characteristics of OSCs, the space charge-limited current (SCLC) method was employed. The resulting hole mobility (μ_h) and electron mobility (μ_e) profiles are presented in Figure S10, with a detailed summary provided in Table S4. The calculated μ_h/μ_e for the PM6:D-TPh and PM6:D-TNbased devices are $8.73\times10^{-4}/8.30\times10^{-4}$ and $8.20\times10^{-4}/7.59\times10^{-4}$ cm^2 V^{-1} s^{-1}, respectively. The PM6:D-TPh device exhibits a more balanced electron and hole mobility ratio, accounting for the improved J_{sc} and FF.

Morphology Analysis

To examine the surface characteristics, atomic force microscopy (AFM) was utilized. As shown in Figure 4a and Figure S11, the two blend films exhibit smooth and uniform surface, along with discernible fibrillar patterns.[40] The root-mean-square roughness (RMS) for the blend films of PM6:D-TPh and PM6:D-TN were measured to be 1.20 and 2.13 nm, respectively. The comparatively smaller RMS of the PM6:D-TPh blend films suggests an effective well-intermixed morphology.

To further analyze the molecular orientation and packing of the neat and blend films, grazing-incidence wide-angle X-ray scattering (GIWAXS) techniques were employed. Figure S12a, 10 b and Figure 4b, Figure S13 for both the neat and blend films depict the 2D-GIWAXS patterns and the corresponding line-cut profiles, representing the in-plane (IP) and out-of-plane (OOP) orientations. Detailed quantitative analyses of the scattering peaks are summarized in Table S5. In neat films, the GIWAXS pattern for PM6 reveals a coexistence of both face-on and edge-on molecular orientations. D-TPh and D-TN both exhibit preference for face-on orientations, as indicated by the distinct π–π (010) stacking diffraction peaks observed at q_z values of 1.52 and 1.55 Å^{-1}, corresponding to π–π distances of 4.13 and 4.11 Å, respectively. Furthermore, the crystalline coherence length (CCL) associated with the π–π stacking peak of D-TPh is

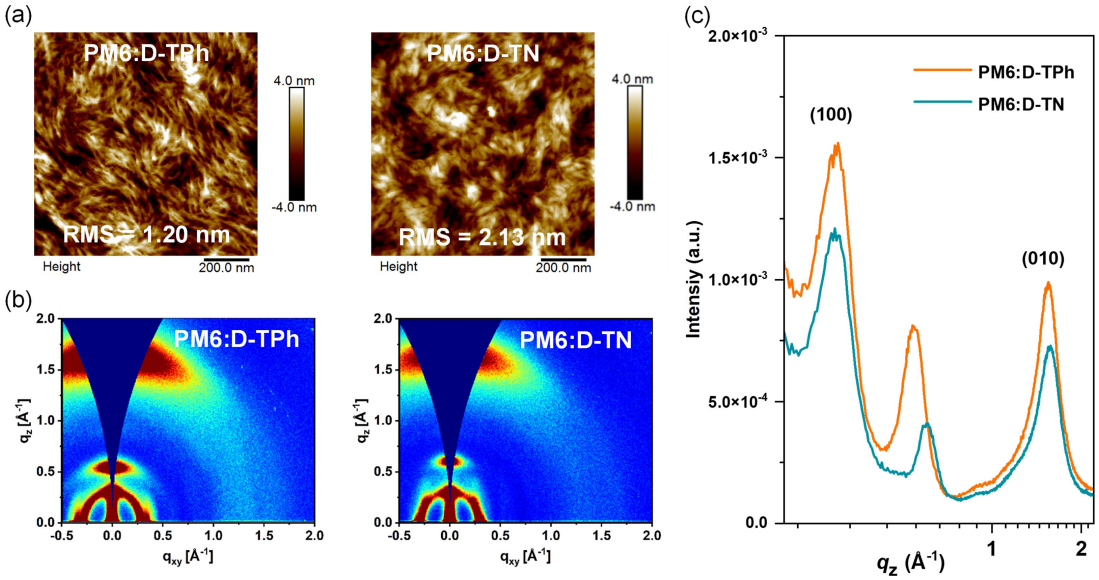

Figure 4. (a) AFM height images (1 μm ×1 μm) of PM6 : D-TPh and PM6 : D-TN blends; (b) 2D GIWAXS patterns of PM6 : D-TPh and PM6 : D-TN blends; (c) The corresponding out-of-plane line-cuts of PM6 : D-TPh and PM6 : D-TN blends.

15.71 Å, higher than that (14.88 Å) of D-TN, suggesting more compact molecular arrangement and enhanced crystallinity for D-TPh compared to D-TN. In terms of blend films, it is noteworthy that all exhibit distinct (010) π–π stacking peaks are evident in both IP and OOP directions. For the two dimeric acceptors, the π–π stacking peaks are consistently positioned at approximately 1.54 Å^{-1}, which implies a similar π–π distance of around 4.0 Å. Furthermore, the calculated CCLs for the (010) peak in the OOP direction are 16.63 Å for PM6 : D-TPh and 16.16 Å for PM6 : D-TN. Notably, the blend film of PM6 : D-TPh demonstrates a significantly stronger (100), and (010) peak intensities in comparison with PM6 : D-TN (Figure 4c). In conclusion, the minor variations in the chemical structures of these dimerized acceptors significantly influence the film's morphology and overall performance of the devices.

To investigate the film formation process, in-situ UV/Visible absorption measurements were performed using chloroform as the solvent. The aggregation of PM6 and D-TPh and D-TN was monitored by observing changes in the intensity of their respective absorption peaks. As illustrated in Figure 5a–d, the film formation process is arbitrarily divided into three distinct stages: solvent evaporation, nucleation and crystal growth, and the formation of a dried film. Both D-TPh and D-TN demonstrated a significant increase in absorption intensity at approximately 188 ms, indicating the onset of aggregation. Concurrently, the intensity of the donor PM6 remained relatively unchanged at the same time, suggesting that acceptor aggregation initiates before that of donor during the film formation. In the PM6 : D-TN sample, D-TN underwent rapid crystallization, especially during the nucleation and crystal growth stages, occurring between 189 and 378 ms. Conversely, in the PM6 : D-TPh sample, the crystallization of the acceptor components was observed to decelerate over a more extended period, from 188 to 441 ms. Thus, the extend the crystallization time of the acceptor is essential for facilitating phase separation and achieving the desired molecular orientation in the resultant film.[41]

Enhancing the stability of OSCs is essential for their widespread commercial use. In this regard, the stability of these devices with MPP tracking under continuous one-sun illumination has been thoroughly investigated. Figure S14 illustrates that the PM6 : D-TN device experiences notable efficiency decay under light exposure, having a T_{80} of 600 h. In contrast, the device based on PM6 : D-TPh demonstrates a reduction in efficiency loss, with its operational lifetime notably extended to 1300 h, which retains over 85 % of its initial PCE. Additionally, by extrapolating the measured photostability data, we estimate a T_{80} lifetime of over 2800 h. Furthermore, the thermal stability of the devices was also examined. The PM6 : D-TN device maintains 79.48 % of its initial PCE after being subjected to 80 °C in an inert atmosphere for 400 h. In comparison, the PCE of PM6 : D-TPh device remains at 84.38 % under the same time. After 680 h of continuous heating, it declines to 80.01 % of its initial PCE. To delve into the thermal stability of these devices, we assessed the T_g of D-TPh and D-TN using UV/Vis absorption measurements at varying temperatures. As depicted in Figure S14, D-TPh and D-TPN have high T_g values of 236 °C and 227 °C, respectively, which contributes to the good photo/thermal stability of the OSCs.

Conclusion

We designed and synthesized two dimer acceptor isomers, D-TPh and D-TN to study the impact of positional arrangement of the end capping groups on molecular conformations, electrical and optical properties, material aggregation,

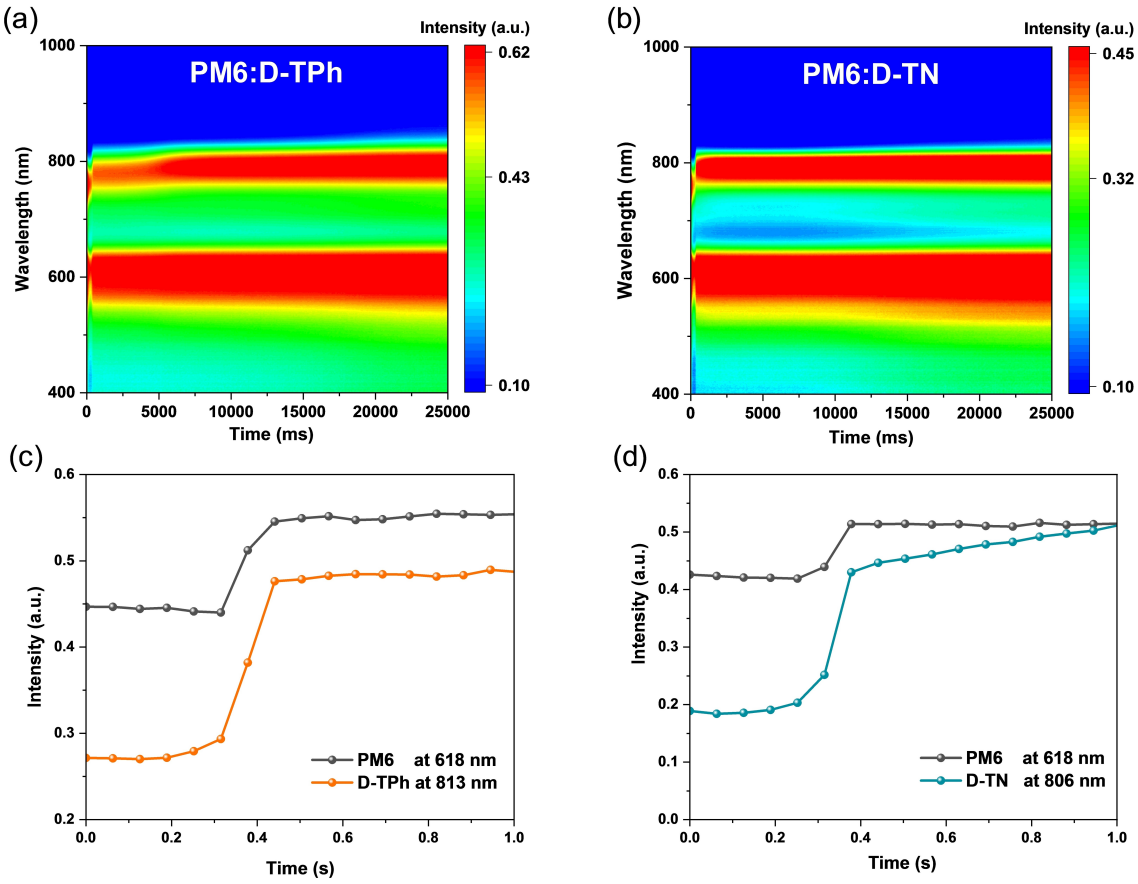

Figure 5. Time-dependent UV/Vis absorption contours of blend films for PM6:D-TPh (a) and PM6:D-TN (b). The evolution of peak intensities and positions for PM6:D-TPh blend films (c), and for PM6:D-TN blend films (d), as extracted from (a) and (b).

crystallization properties, and photovoltaic performance. D-TPh, featuring reduced conjugate lengths on the thiophene-like sides, exhibits enhanced planarity, elevated LUMO level, and improved molecular packing. As a result, the OSC based on PM6:D-TPh exhibited a high PCE of 19.05 %. Additionally, PM6:D-TPh device showed significant improvements in efficiency retention, with a T_{80} lifetime exceeding 2800 h under continuous one-sun illumination and a retention over 80 % of its initial efficiency after being subjected to 80 °C for 680 h. These findings underscore the effectiveness of the isomerization strategy in the rational design of dimer acceptors, which can significantly contribute to the development of high-efficiency and stable OSCs.

Supporting Information

Supporting Information is available from the Wiley Online Library or the author.

Acknowledgements

This work was financially supported by the National Natural Science Foundation of China (Grant No. 52333005), the Beijing Natural Science Foundation (Z230018), Zhejiang Provincial Natural Science Foundation of China (LZ23B040001), and Interdisciplinary Research Project of Hangzhou Normal University (2024JCXK05).

Conflict of Interest

The authors declare no conflict of interest.

Data Availability Statement

The data that support the findings of this study are available from the corresponding author upon reasonable request.

Keywords: Organic solar cells · Dimer acceptors · Isomeric engineering · High Efficiency · Long-term stability

[1] M. Kaltenbrunner, M. S. White, E. D. Głowacki, T. Sekitani, T. Someya, N. S. Sariciftci, S. Bauer, *Nat. Commun.* **2012**, *3*, 770.
[2] G. Li, R. Zhu, Y. Yang, *Nat. Photonics* **2012**, *6*, 153–161.
[3] S.-Y. Chang, P. Cheng, G. Li, Y. Yang, *Joule* **2018**, *2*, 1039–1054.
[4] K. Fukuda, K. Yu, T. Someya, *Adv. Energy Mater.* **2020**, *10*, 2000765.

[5] W. Huang, Z. Jiang, K. Fukuda, X. Jiao, C. R. McNeill, T. Yokota, T. Someya, *Joule* **2020**, *4*, 128–141.
[6] L. Zhu, M. Zhang, J. Xu, C. Li, J. Yan, G. Zhou, W. Zhong, T. Hao, J. Song, X. Xue, Z. Zhou, R. Zeng, H. Zhu, C.-C. Chen, R. C. I. MacKenzie, Y. Zou, J. Nelson, Y. Zhang, Y. Sun, F. Liu, *Nat. Mater.* **2022**, *21*, 656–663.
[7] S. Luo, C. Li, J. Zhang, X. Zou, H. Zhao, K. Ding, H. Huang, J. Song, J. Yi, H. Yu, K. S. Wong, G. Zhang, H. Ade, W. Ma, H. Hu, Y. Sun, H. Yan, *Nat. Commun.* **2023**, *14*, 6964.
[8] J. Song, C. Zhang, C. Li, J. Qiao, J. Yu, J. Gao, X. Wang, X. Hao, Z. Tang, G. Lu, R. Yang, H. Yan, Y. Sun, *Angew. Chem. Int. Ed.* **2024**, *63*, e202404297.
[9] M. Ghasemi, N. Balar, Z. Peng, H. Hu, Y. Qin, T. Kim, J. J. Rech, M. Bidwell, W. Mask, I. McCulloch, W. You, A. Amassian, C. Risko, B. T. O'Connor, H. Ade, *Nat. Mater.* **2021**, *20*, 525–532.
[10] N. Li, J. D. Perea, T. Kassar, M. Richter, T. Heumueller, G. J. Matt, Y. Hou, N. S. Güldal, H. Chen, S. Chen, S. Langner, M. Berlinghof, T. Unruh, C. J. Brabec, *Nat. Commun.* **2017**, *8*, 14541.
[11] Q. Burlingame, M. Ball, Y.-L. Loo, *Nat. Energy* **2020**, *5*, 947–949.
[12] C. Zhang, J. Song, L. Ye, X. Li, M. H. Jee, H. Y. Woo, Y. Sun, *Angew. Chem. Int. Ed.* **2024**, *63*, e202316295.
[13] H. Zhuo, X. Li, J. Zhang, S. Qin, J. Guo, R. Zhou, X. Jiang, X. Wu, Z. Chen, J. Li, L. Meng, Y. Li, *Angew. Chem. Int. Ed.* **2023**, *62*, e202303551.
[14] J. Wu, Z. Ling, L. R. Franco, S. Y. Jeong, Z. Genene, J. Mena, S. Chen, C. Chen, C. M. Araujo, C. F. N. Marchiori, J. Kimpel, X. Chang, F. H. Isikgor, Q. Chen, H. Faber, Y. Han, F. Laquai, M. Zhang, H. Y. Woo, D. Yu, T. D. Anthopoulos, E. Wang, *Angew. Chem. Int. Ed.* **2023**, *62*, e202302888.
[15] Y. Liang, D. Zhang, Z. Wu, T. Jia, L. Lüer, H. Tang, L. Hong, J. Zhang, K. Zhang, C. J. Brabec, N. Li, F. Huang, *Nat. Energy* **2022**, *7*, 1180–1190.
[16] C. Wang, X. Ma, Y.-f. Shen, D. Deng, H. Zhang, T. Wang, J. Zhang, J. Li, R. Wang, L. Zhang, Q. Cheng, Z. Zhang, H. Zhou, C. Tian, Z. Wei, *Joule* **2023**, *7*, 2386–2401.
[17] H. Wang, C. Cao, H. Chen, H. Lai, C. Ke, Y. Zhu, H. Li, F. He, *Angew. Chem. Int. Ed.* **2022**, *61*, e202201844.
[18] J.-W. Lee, C. Sun, C. Lee, Z. Tan, T. N.-L. Phan, H. Jeon, D. Jeong, S.-K. Kwon, Y.-H. Kim, B. J. Kim, *ACS Energy Lett.* **2023**, *8*, 1344–1353.
[19] Y. Bai, Z. Zhang, Q. Zhou, H. Geng, Q. Chen, S. Kim, R. Zhang, C. Zhang, B. Chang, S. Li, H. Fu, L. Xue, H. Wang, W. Li, W. Chen, M. Gao, L. Ye, Y. Zhou, Y. Ouyang, C. Zhang, F. Gao, C. Yang, Y. Li, Z.-G. Zhang, *Nat. Commun.* **2023**, *14*, 2926.
[20] M. Zhang, B. Chang, R. Zhang, S. Li, X. Liu, L. Zeng, Q. Chen, L. Wang, L. Yang, H. Wang, J. Liu, F. Gao, Z.-G. Zhang, *Adv. Mater.* **2024**, *36*, 2308606.
[21] F. Qi, Y. Li, R. Zhang, F. R. Lin, K. Liu, Q. Fan, A. K. Y. Jen, *Angew. Chem. Int. Ed.* **2023**, *62*, e202303066.
[22] F. Cheng, Y. Cui, F. Ding, Z. Chen, Q. Xie, X. Xia, P. Zhu, X. Lu, H. Zhu, X. Liao, Y. Chen, *Adv. Mater.* **2023**, *35*, 2300820.
[23] T. Xu, Z. Luo, R. Ma, Z. Chen, T. A. Dela Peña, H. Liu, Q. Wei, M. Li, C. e Zhang, J. Wu, X. Lu, G. Li, C. Yang, *Angew. Chem. Int. Ed.* **2023**, *62*, e202304127.
[24] Z. Luo, T. Liu, H. Yan, Y. Zou, C. Yang, *Adv. Funct. Mater.* **2020**, *30*, 2004477.
[25] C. Han, H. Jiang, P. Wang, L. Yu, J. Wang, J. Han, W. Shen, N. Zheng, S. Wen, Y. Li, X. Bao, *Mater. Chem. Front.* **2021**, *5*, 3050–3060.
[26] G. Kupgan, X.-K. Chen, J.-L. Brédas, *ACS Appl. Energ. Mater.* **2021**, *4*, 4002–4011.
[27] C. Yang, Q. An, M. Jiang, X. Ma, A. Mahmood, H. Zhang, X. Zhao, H. F. Zhi, M. H. Jee, H. Y. Woo, X. Liao, D. Deng, Z. Wei, J. L. Wang, *Angew. Chem. Int. Ed.* **2023**, *62*, e202313016.
[28] T. Lin, Y. Hai, Y. Luo, L. Feng, T. Jia, J. Wu, R. Ma, T. A. Dela Peña, Y. Li, Z. Xing, M. Li, M. Wang, B. Xiao, K. S. Wong, S. Liu, G. Li, *Adv. Mater.* **2024**, *36*, 2312311.
[29] C. Zhang, J. Li, W. Deng, J. Dai, J. Yu, G. Lu, H. Hu, K. Wang, *Adv. Funct. Mater.* **2023**, *33*, 2301108.
[30] T. Wang, R. Sun, W. Wang, H. Li, Y. Wu, J. Min, *Chem. Mater.* **2021**, *33*, 761–773.
[31] M. Deng, X.-P. Xu, L.-Y. Yu, R.-P. Li, Q. Peng, *Chin. J. Polym. Sci.* **2022**, *40*, 928–936.
[32] M. Luo, Y. Chen, J. Liang, J. Zhou, D. Yuan, Z. Zhang, X. Liu, L. Zhang, Z. Xie, J. Chen, *ACS Appl. Mater. Interfaces* **2022**, *14*, 35985–35996.
[33] Z. Chen, J. Zhu, D. Yang, W. Song, J. Shi, J. Ge, Y. Guo, X. Tong, F. Chen, Z. Ge, *Energy Environ. Sci.* **2023**, *16*, 3119–3127.
[34] Y. Zhu, X. Shen, H. Lai, M. Pu, Y. Zhu, X. Lai, S. Xiong, F. He, *Nano Energy* **2023**, *118*, 108991.
[35] X. Gu, X. Zhang, H. Huang, *Angew. Chem. Int. Ed.* **2023**, *135*, e202308496.
[36] F. Qi, Y. Li, R. Zhang, F. R. Lin, K. Liu, Q. Fan, A. K.-Y. Jen, *Angew. Chem. Int. Ed.* **2023**, *62*, e202303066.
[37] C. Sun, J.-W. Lee, C. Lee, D. Lee, S. Cho, S.-K. Kwon, B. J. Kim, Y.-H. Kim, *Joule* **2023**, *7*, 416–430.
[38] P. W. M. Blom, V. D. Mihailetchi, L. J. A. Koster, D. E. Markov, *Adv. Mater.* **2007**, *19*, 1551–1566.
[39] L. J. A. Koster, V. D. Mihailetchi, R. Ramaker, P. W. M. Blom, *Appl. Phys. Lett.* **2005**, *86*, 123509.
[40] T. Xia, Y. Cai, H. Fu, Y. Sun, *Sci. China Chem.* **2019**, *62*, 662–668.
[41] Z. Peng, Y. Zhang, X. Sun, W. Zhao, F. Bian, Y. Geng, L. Ye, C. Yang, *Adv. Funct. Mater.* **2023**, *33*, 2213248.

Manuscript received: June 12, 2024
Accepted manuscript online: September 5, 2024
Version of record online: October 29, 2024